The influence of surface tension gradients on drop coalescence

Citation: Blanchette, Francois, Laura Messio, and John W. M. Bush. "The influence of surface tension gradients on drop coalescence." Physics of Fluids 21.7 (2009): 072107-10. © 2009 American Institute of Physics

As Published: http://dx.doi.org/10.1063/1.3177339

Publisher: American Institute of Physics

Persistent URL: http://hdl.handle.net/1721.1/58728

Version: Final published version: final published article, as it appeared in a journal, conference proceedings, or other formally published context

The influence of surface tension gradients on drop coalescence

François Blanchette,[1] Laura Messio,[2] and John W. M. Bush[2]
[1]*School of Natural Sciences, University of California Merced, 5200 N. Lake Rd., Merced, California 95343, USA*
[2]*Department of Mathematics, Massachusetts Institute of Technology, 77 Massachusetts Ave., Cambridge, Massachusetts 02139, USA*

(Received 6 November 2008; accepted 22 June 2009; published online 21 July 2009)

We present the results of a combined experimental and numerical investigation of the coalescence of a drop with a liquid reservoir of a miscible but distinct fluid. Particular attention is given to elucidating the influence on the coalescence process of a surface tension difference between drop and reservoir. Drops are gently deposited on the surface of the reservoir, and so coalesce with negligible initial vertical velocity. Depending on the drop size and reservoir composition, partial or total coalescence may occur. Three distinct regimes, depending on the reservoir to drop surface tension ratio, R_σ, are identified and delineated through both experiments and numerics. If $R_\sigma < 0.42$, droplets are ejected from the top of the drop, while satellite droplets are left in its wake. For $0.42 \leq R_\sigma < 0.93$, only total coalescence is observed. When $R_\sigma \geq 0.93$, partial coalescence is increasingly favored as the reservoir's surface tension increases. © *2009 American Institute of Physics*. [DOI: 10.1063/1.3177339]

I. INTRODUCTION

The coalescence of a droplet into a reservoir of like fluid has been studied in the context of emulsions,[1] raindrop formation[2] and, more recently, microfluidic devices.[3,4] The mixing that results from drop coalescence has received particular attention owing to its importance in both natural and industrial settings.[5,6] The advent of fast cameras and powerful numerical simulations has shed new light on the details of droplet coalescence. In particular, the phenomenon of partial coalescence, first reported almost 50 years ago,[7,8] has received considerable recent attention.

When a drop is gently placed on a reservoir of the same fluid, gravity draws the drop downward and eventually the drop and reservoir interfaces become sufficiently close ($\sim$100 nm) that attractive Van der Waals forces initiate coalescence. The resulting fluid neck that joins them rapidly opens up; moreover, in the inertia-dominated regime of interest here, capillary waves propagate away from the initial point of contact. Two very different outcomes may follow: Either total coalescence occurs and the drop merges entirely with the reservoir, or only a fraction of the drop liquid merges with the reservoir and a daughter drop is left behind. For partial coalescence to occur, the horizontal constriction of the interface, driven by the surface tension on the sides of the drops, must overcome the vertical collapse driven by the curvature at the top of the drop. When capillary waves are able to reach the drop's summit before being damped, they interfere with the vertical collapse and allow the horizontal pull of surface tension to prevail and cause pinch-off of the interface.[9] The daughter drop left behind by partial coalescence is projected downward, bounces on the reservoir surface, and eventually comes to rest before undergoing a similar process, yielding a coalescence cascade. When the daughter drop becomes sufficiently small, viscous effects come into play and total coalescence occurs.

In the inertially dominated regime relevant to liquids of low viscosity[10] determined that the dominant forces at play were surface tension and inertia, and the characteristic time scale of coalescence $\tau=(\rho R^3/\sigma)^{1/2}$, where R is the drop radius, ρ is its density, and σ is the surface tension. The critical role of capillary waves in partial coalescence was identified by Chen *et al.*[11] (2006) and criteria for partial coalescence in air-liquid systems were presented by Blanchette and Bigioni[9] in 2006. A mechanism for partial coalescence relying on the presence of surfactants was also presented.[12] Subsequent experimental studies have elucidated further details of the coalescence process including the existence of a viscously dominated partial coalescence regime.[13–15]

We examine here the influence on the coalescence process of a surface tension difference, as may arise from differences in temperature or composition, between drop and reservoir. The influence of Marangoni effects, or equivalently surface tension gradients,[16,17] on droplet coalescence has received very little attention. Coalescence in the presence of an initially uniform concentration of surfactants was investigated[18,19] with a particular focus on residence times and on the evolution of the thin film separating the drop from the reservoir, but no systematic surface tension gradients were introduced. It was later demonstrated that drop coalescence may be delayed by a temperature gradient between drop and reservoir[20,21] since the resulting Marangoni stresses may serve to resist the drainage of the intervening air layer. The early stages of the coalescence of a drop held by a tube and of composition different from that of the underlying reservoir were recently visualized using an extremely fast camera.[22] However, the coalescence of a freestanding, initially quiescent drop in the presence of Marangoni stresses has yet to be investigated. In particular, the conditions under which the coalescence is partial or total have yet to be determined. A direct application of inhomogeneous drop coales-

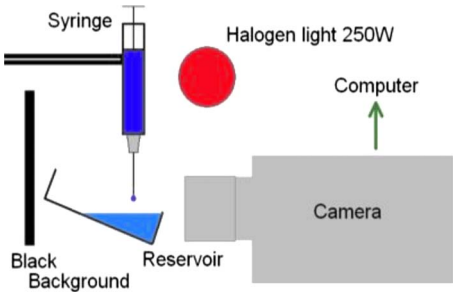

FIG. 1. (Color online) Schematic of the experiment: The drop is released from a syringe and falls onto a reservoir bound in an inclined container. The coalescence process is observed with a high-speed camera.

cence was recently suggested as a sorting mechanism for drops on a vertically vibrated reservoir:[23] Drops larger than a given threshold undergo partial coalescence while smaller drops bounce indefinitely on the interface.[24]

In Sec. II, we present the results of our experimental study. The governing equations are developed in Sec. III, and our numerical model described in Sec. IV. In Sec. V, we present the results of our numerical investigation, and in Sec. VI we use them to rationalize the observations reported in Sec. II. Our principal conclusions are presented in Sec. VII along with a discussion of directions for future research.

II. EXPERIMENTS

We examine the coalescence of a droplet brought by gravity into contact with a liquid reservoir of different compositions. To highlight the effects of surface tension variations while minimizing those of density and viscosity, we used water-ethanol mixtures for both the drop and reservoir fluids. This also ensured that coalescence took place in an inertially dominated regime so that the early neck expansion remained stable to the a previously reported instability.[25]

A schematic representation of the experimental apparatus is shown in Fig. 1. Drops were generated by manually pressing on a syringe, located 6 mm above the reservoir, and detached when their weight overcame surface forces. The radius, R, of the resulting drops typically ranged between 1.2 and 1.5 ± 0.1 mm, depending on their composition. The coalescence of the initial drop typically lasted approximately 0.01 s and each coalescence event was recorded using a 3000 frames/s high speed camera (Phantom V7.5). When partial coalescence occurred, up to five generations of daughter droplets were observed but only the first coalescence was examined, as the composition of the daughter droplet and the underlying bath could not be accurately determined thereafter. The container was inclined to avoid difficulties associated with focusing across the glass. To eliminate contamination and temperature gradients, the solutions were replenished after each experiment.

To reduce the number of parameters influencing the coalescence process, we focus on drops that are virtually immobile at the onset of coalescence and for which the reservoir interface is nearly flat. While the former condition is relatively easily met when the composition of the drop and reservoir are identical, we found that drops of different compositions tended to initiate coalescence before coming to rest. After leaving the syringe, such drops often coalesced upon first contact with the reservoir or while rebounding, thus initiating coalescence with a significant downward or upward velocity, respectively. This short rest time may be due to the condensation of ethanol vapor into either the drop or reservoir, thereby creating on the interface an area of lower surface tension. Tangential flow away from the point of contact then tends to drive air out of the gap between drop and reservoir, and reduce the time the drops spends above he interface before coalescence.[26] Obtaining reproducible initial conditions was thus proved challenging and limited the scope of our experimental observations. The drop and reservoir fluids were made of either pure water, pure ethanol, or one of five ethanol-water mixtures, as shown in Table I. The viscosity was calculated based on the results of Ref. 27 and the density measured with an Anton–Parr densitometer. The surface tension was measured using the Wilhemy method with a Kruss K10 tensiometer.

TABLE I. The mixtures used in our experiments.

Mix No.	Ethanol fraction (%)	Surface tension (mN/m)	Density (g/cm^3)	Viscosity (cP)
0	100 ± 0.5	22.0 ± 0.1	0.7851 ± 10^{-4}	1.10 ± 0.02
1	60	27.2	0.8895	2.24
2	55	27.7	0.9010	2.29
3	50	28.8	0.9125	2.33
4	40	30.3	0.9342	2.34
5	30	33.4	0.9535	2.13
6	0	73.0	1.000	0.893

We consider a drop of density ρ_1, viscosity $\mu_1 = \rho_1 \nu_1$, and surface tension σ_1, overlying a reservoir of density ρ_2 and viscosity μ_2, and most importantly with different surface tensions σ_2. The surrounding air has density ρ_{gas}. The compositional diffusivity of alcohol in the alcohol-water solutions comprising the drop and reservoir fluid is given by κ. To focus on the effects of surface tension gradients, we assume in our analysis that $\mu_1 = \mu_2 = \mu_l$ and $\rho_1 = \rho_2 = \rho_l$, and find that four dimensionless numbers characterize the system,

$$\text{Bo} = \frac{(\rho_l - \rho_{\text{gas}})gR^2}{\sigma_1}, \tag{1}$$

$$\text{Sc} = \frac{\nu_l}{\kappa}, \tag{2}$$

$$\text{Oh} = \frac{\mu_l}{\sqrt{\rho_l R \sigma_1}}, \tag{3}$$

$$R_\sigma = \frac{\sigma_2}{\sigma_1}. \tag{4}$$

The Bond number, Bo, prescribes the relative magnitudes of the gravitational potential and surface energies of the drop. The Schmidt number, Sc, prescribes the relative magnitudes of the diffusivities of momentum and composition. The Ohnesorge number, Oh, prescribes the relative importance of

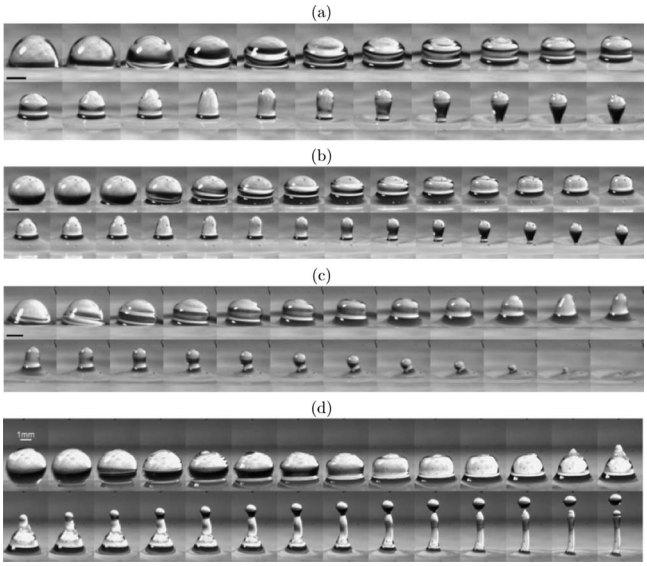

FIG. 2. Time sequences of four coalescence events for different pairs of fluids. Each frame is separated by 0.33 ms and the scale bar is 1 mm. Following the notation of Table I, the reservoir and drop are (a) solution 4 and solution 2 ($R_\sigma=\sigma_2/\sigma_1=1.09$), (b) solution 4 and solution 4 ($R_\sigma=1$), (c) solution 4 and solution 5 ($R_\sigma=0.91$), and (d) solution 0 and solution 6 ($R_\sigma=0.30$), respectively. In both (a) and (b) a downward moving daughter drop was formed. In (c) the coalescence was total and in (d) a small daughter drop was ejected upward.

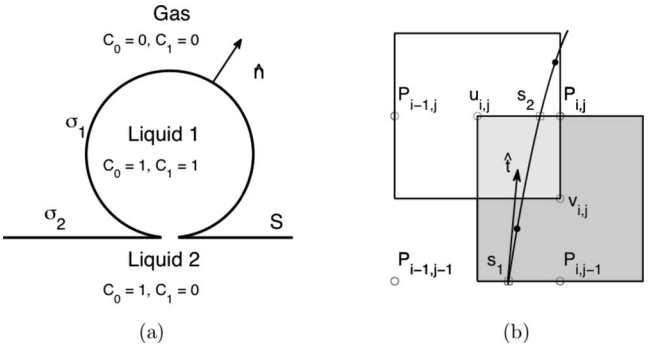

FIG. 3. (a) Initial configuration of a drop of liquid 1 at rest on a reservoir of liquid 2. Simulations are initiated at the onset of coalescence, with a thin neck joining the drop and reservoir. Initial values of the concentration functions C_0 and C_1 are shown. (b) Staggered grid used, shown around the point where $v_{i,j}$ is defined. The black curve is the interface, interpolated between markers (black dots).

viscous stresses and curvature pressures. We focus here on the inertial regime, $\mathrm{Oh}\ll 1$, where partial coalescence is known to take place.[10] Finally, the surface tension ratio, R_σ, is the key parameter of our study and its influence on the coalescence process had yet to be considered. In our experiments, the first three nondimensional numbers were kept nearly constant, with $\mathrm{Bo}\approx 0.2$, $\mathrm{Sc}\approx 800$, and $\mathrm{Oh}\approx 0.01$, while the surface tension ratio was varied systematically in the range of $0.3\leq R_\sigma\leq 3.3$.

For $R_\sigma=1$, we observed a coalescence cascade analogous to that reported in Refs. 7–10, see Fig. 2(b). For $R_\sigma>1$, the coalescence was also partial for drops of sufficiently small Ohnesorge numbers, and qualitatively similar to the $R_\sigma=1$ case, Fig. 2(a). The resulting daughter drop appeared slightly larger than for the $R_\sigma=1$ case and itself proceeded to undergo partial coalescence. The entire coalescence cascade showed little variation from the $R_\sigma=1$ case.

More complex behavior was observed for $R_\sigma<1$. For $R_\sigma>0.94$, partial coalescence still developed in a manner similar to the $R_\sigma=1$ case. However, for $0.42<R_\sigma<0.94$, total coalescence was always observed, see Fig. 2(c). For $R_\sigma<0.42$, a new type of partial coalescence arose [Fig. 2(d)]. The early stages resembled those of the classic partial coalescence, with the lower neck rapidly opening, the formation of capillary waves on the interface and the vertical stretching of the drop. The stretching, however, was seen to be much more pronounced than when $R_\sigma=1$. The top of the drop formed a nearly cylindrical column that rose under the influence of the Marangoni stresses, while fluid in the lower regions of the drop drained into the lower reservoir. Eventually, the column of fluid ejected a droplet from its summit. This upward ejection was a robust, repeatable effect. The ejected droplet was approximately 2.5–3.5 times smaller in radius than the mother drop, with smaller drops arising from larger surface tension differences. Unlike daughter drops normally seen in partial coalescence, which are moving downward at the time of pinch-off, the daughter droplet was ejected vertically upward, and its ejection speed increased with surface tension contrast. In the most extreme setup considered [Fig. 2(d)], a water drop on a pure ethanol bath, the droplet rose up to the height of the syringe (6 mm above the reservoir). The ejection also gave rise to smaller satellite droplets that formed between the column of fluid and the ejected droplet. Contrary to daughter droplets formed by the classic partial coalescence of drops surrounded by gas, the ejected droplets, once brought downward by gravity, did not bounce on the reservoir surface, but instead coalesced immediately with the underlying bath.

It is worth emphasizing that such ejection events do not result from converging capillary waves that are known to generate microjets in various circumstances, including bursting bubbles,[28] oscillating satellite drops,[29] drops impacting a solid surface,[30] liquid crater collapse,[31] and the coalescence of drops at large Bond numbers.[32] Rather than converging waves, here the ejection is generated by the converging tangential motion along the interface. This motion entrains a significant quantity of fluid, which leads to the formation of daughter droplets of size comparable to that of the mother drop.

III. GOVERNING EQUATIONS

To model our experiments, we consider a drop of liquid 1 slowly coming into contact with a reservoir of liquid 2 while surrounded by air (Fig. 3). The two liquids are miscible with identical density, ρ_l, and viscosity, μ_l, but may have different surface tensions. To describe this multiphase system, we first introduce a concentration function, C_0, that describes the relative fraction of liquid at a given point, with $C_0=0$ in the air and $C_0=1$ in either liquid. The position of the interface, S, determines the value of C_0 at any point. We also introduce a concentration function, C_1, describing the

proportion of liquid 1 relative to liquid 2 at a point, with $C_1=0$ in pure liquid 2 and $C_1=1$ in pure liquid 1.

We may write expressions for the viscosity $\mu(C_0)$ and density $\rho(C_0)$ at every point in the domain. The surface tension, $\sigma(C_1)$, is only defined on the interface and is therefore independent of C_0. Following several earlier authors,[33–35] we model the interface as a forcing term, F_s, which we add to the momentum equation of the Navier–Stokes equations. Assuming all fluids to be incompressible, the governing equations for our system are

$$\rho(\vec{u}_t + \vec{u}\cdot\nabla\vec{u}) = -\nabla p + \nabla\cdot\{\mu[\nabla\vec{u} + (\nabla\vec{u})^T]\} + \rho g + F_s, \tag{5}$$

$$\nabla\cdot\vec{u} = 0, \tag{6}$$

$$S_t = \vec{u}, \tag{7}$$

$$(C_1)_t + \vec{u}\cdot\nabla C_1 = \nabla\cdot(\kappa\nabla C_1), \tag{8}$$

where $\vec{u}$ is the velocity field, p is the pressure, f_t denotes the time derivative of f, κ is the compositional diffusivity, which generally depends on C_1, and the interface position is defined by S. Equations (5) and (6) describe the evolution of the momentum and mass of incompressible fluids. Equation (7) states that the interface moves with the flow and that no evaporation or condensation is taking place. Finally, Eq. (8) describes the evolution of the concentration C_1 under the combined influence of fluid advection and molecular diffusion.

The forcing term F_s is a surface delta function that is nonzero only on the interface,[34–36]

$$F_s = \delta(S)\nabla\cdot[(\bar{\bar{I}} - \hat{n}^T\hat{n})\sigma] = \delta(S)(\nabla_S\sigma + 2\kappa_m\hat{n}\sigma), \tag{9}$$

where $\hat{n}$ is a unit normal to the surface, $\bar{\bar{I}}-\hat{n}^T\hat{n}$ is a projection operator, ∇_S is a gradient operator defined on the interface, $\kappa_m=\frac{1}{2}\nabla\cdot\hat{n}$ is the mean curvature of the interface, and $\delta(S)$ is defined such that

$$\int\int\int_V \delta(S)f(\vec{x})dV = \int\int_S f(\vec{x})dS$$

for any smooth test function $f(\vec{x})$. The forcing term therefore captures the normal component of curvature-induced stress, as well as the tangential component resulting from surface tension gradients. Using such a formulation is equivalent to enforcing normal and tangential stress conditions on the interface, but has proven to be much more efficient to implement in simulations.

We nondimensionalize the governing equations using the drop radius, R, as a length scale, $\tau=(\rho_l R^3/\sigma_1)^{1/2}$, as a time scale, with σ_1 the drop surface tension of the drop, to find

$$\rho'(\vec{u}_t + \vec{u}\cdot\nabla\vec{u}) = -\nabla p + \mathrm{Oh}\ \nabla\cdot\{\mu'[\nabla\vec{u} + (\nabla\vec{u})^T]\} + \rho'\ \mathrm{Bo} + \delta(S)\nabla\cdot[(\bar{\bar{I}} - \hat{n}^T\hat{n})\sigma'], \tag{10}$$

$$\nabla\cdot\vec{u} = 0, \tag{11}$$

$$S_t = \vec{u}, \tag{12}$$

$$(C_1)_t + \vec{u}\cdot\nabla C_1 = (\mathrm{Oh}/\mathrm{Sc})\nabla\cdot(\kappa'\nabla C_1), \tag{13}$$

where all variables are now dimensionless and $\mu'=\mu/\mu_l$, $\rho'=\rho/\rho_l$, $\kappa'=\kappa/\kappa_1$, and $\sigma'=\sigma/\sigma_1$, and the dimensionless numbers Bo, Oh, and Sc are as defined in Sec. II. For simplicity, the hydrostatic pressure of the gas was incorporated into the pressure term so that p now represents a dynamic pressure. Note that Eq. (8) describes the evolution of miscible fluids as well as that of liquids of variable temperature, if C_1 stands for the liquid temperature and κ for the thermal diffusivity.

IV. NUMERICAL SIMULATIONS

The core of the numerical simulations used here is analogous to those described by Blanchette and Bigioni[32] (2009). A fixed staggered grid is used to compute the velocity, concentration, stress, and pressure fields. The projection method is used to compute the pressure[37] and first order corrections are included near the interface to take into account the discontinuity of the pressure across the interface.[35] The interface is tracked using tracer particles that move with the fluid, and cubic splines are used to interpolate between the markers. We consider an axisymmetric cylindrical domain corresponding to a container closed at the top and bottom with the drop aligned on its axis. The boundary conditions imposed on the system are those of no-slip on, and zero flux through, the solid walls, which are positioned sufficiently far from the drop that they do not affect the coalescence process. Our initial conditions consist of a spherical drop at rest just at the point of contact with a horizontal surface: The two surfaces are initially connected by a neck. We follow the evolution of the drop until either the surface comes within a given threshold value of the symmetry axis, at which point we assume that pinch-off occurs, or total coalescence is achieved. A validation of simulations based on the same numerical scheme, but with constant surface tension, was presented in Ref. 32.

We now describe the treatment of the second liquid and its impact on fluid properties and related computations, which have not been described elsewhere. We use linear relationships between the gaseous and liquid fractions, C_0 and C_1, and the density, viscosity, and surface tension. For the density and viscosity we have

$$\rho' = [\rho_{\mathrm{gas}}(1-C_0) + C_0\rho_l]/\rho_l,$$

$$\mu' = [\mu_{\mathrm{gas}}(1-C_0) + C_0\mu_l]/\mu_l,$$

where subscripts l and "gas" indicate properties of the pure liquid and of the gas, respectively. In the case of surface tension, only the concentration in the liquid phase is taken into account,

$$\sigma' = [\sigma_2(1-C_1) + \sigma_1 C_1]/\sigma_1 = R_\sigma(1-C_1) + C_1.$$

To keep the number of parameters to a manageable level while highlighting the effect of the surface tension gradients, we assume that the compositional diffusivity, κ, is independent of C_1.

Blanchette and Bigioni[32] (2009) found that air plays a negligible dynamical role in the system evolution and that

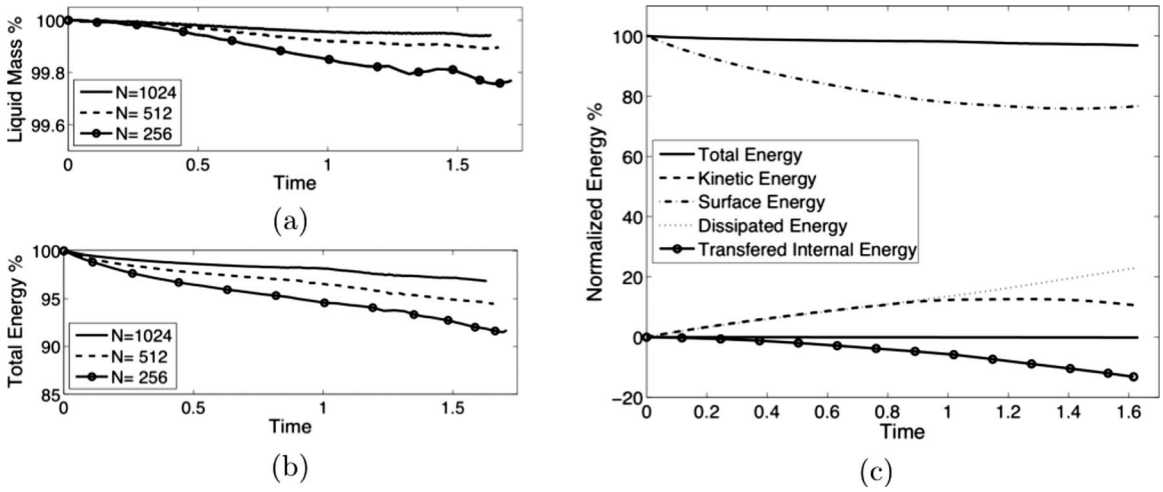

FIG. 4. Time evolution of (a) the liquid mass and (b) the total energy calculated at different resolutions. (c) Evolution of the different energy components enumerated in Eq. (14). System parameters are R_σ=1.17, Oh=0.01, Bo=0, and Sc=50.

overestimating the air density and viscosity did not affect the coalescence outcome provided they remained significantly less than those of the liquid. Moreover, the density and viscosity discontinuities across the interface render the use of the exact air density and viscosity difficult, as mass and energy conservation can only be achieved through the use of an extremely fine resolution.

To allow for faster computations, we therefore fix the air density and viscosity to be 10% those of the drop. While the concentration of air, C_0, is determined solely from the position of the interface, the liquid concentration, C_1, is advanced in time according to Eq. (8). The advection term is computed via an upwinding scheme while the diffusive term is obtained via central differences. We also impose the condition $0 \leq C_1 \leq 1$ directly. Zero-flux boundary conditions are imposed on the solid walls.

To calculate the surface forcing term, we first introduce markers that locate the position of the interface.[35] The velocity of the markers is determined by a bilinear interpolation of the velocity of the surrounding nodes. The position of the markers is then advanced in time using a simple Euler method. Cubic spline interpolations provide an estimate of the interface position between markers. The average surface forcing term per grid cell is then estimated by integrating $\nabla \cdot [(\bar{\bar{I}} - \hat{n}^T \hat{n}) \sigma']$ along the interface. Because our configuration is axially symmetric, the surface force term reduces to (see Ref. 32 for a more detailed derivation in the case of constant σ')

$$(F_s)_{i,j} = \int_{s_1}^{s_2} \sigma' \nabla \cdot (\bar{\bar{I}} - \hat{n}^T \hat{n}) + (\bar{\bar{I}} - \hat{n}^T \hat{n}) \cdot \nabla \sigma' ds$$

$$= \int_{s_1}^{s_2} \sigma' \frac{d\hat{t}}{ds} + \frac{\sigma'}{r} \frac{dy}{ds} + \hat{t} \frac{d\sigma'}{ds} ds$$

$$= \int_{s_1}^{s_2} \frac{d\hat{t}\sigma'}{ds} + \frac{\sigma'}{r} \frac{dy}{ds} ds = \hat{t}\sigma'|_{s_1}^{s_2} + \int_{s_1}^{s_2} \frac{\sigma'}{r} \frac{dy}{ds} ds,$$

where r is the distance to the symmetry axis, y is the vertical coordinate, and s is the arc length. s_1 and s_2 are the intersection points between the curve and the (i,j)th grid cell, and $\hat{t}$ is a unit vector tangent to the curve. The last integral is evaluated numerically by discretizing the interface between markers. Note that $(F_s)_{i,j}=0$ when the curve does not intersect the (i,j)th cell.

V. NUMERICAL RESULTS

A. Validation

In order to focus on the effects of variable surface tension, we kept the Schmidt number constant at $\mathrm{Sc} = \nu_1/\kappa_1 = 50$ to model systems where diffusion of concentration is much slower than that of momentum, such as ethanol-water solutions. Note that using a larger Sc is more computationally demanding and yielded nearly identical results. We also set the Bond number, which characterizes the importance of gravity, to Bo=0, and initiate coalescence when the drop is spherical and the interface is flat. These conditions provide a good approximation of our experiments, where the surface tension variations are dominant.

We begin by verifying the conservation of mass and energy at various resolutions [Fig. 4(a)]. While the liquid mass is well conserved even at fairly low resolutions, the conservation of energy requires higher resolutions. In the presence of spatial surface tension variations for miscible liquids of equal density, and neglecting gravitational effects, the energy evolution was shown to obey[36]

$$\frac{d}{dt}(K + \mathrm{SE}) = -\Phi + \int_S \frac{D\sigma}{Dt} dS, \tag{14}$$

where K and SE are the total kinetic and surface energy of the fluids, respectively, Φ is the rate of energy dissipated through the action of viscosity, and the last term accounts for the transfer from internal to surface energy, as the diffusion of C_1, from the bulk of the drop and reservoir to the interface, affects the local surface tension.

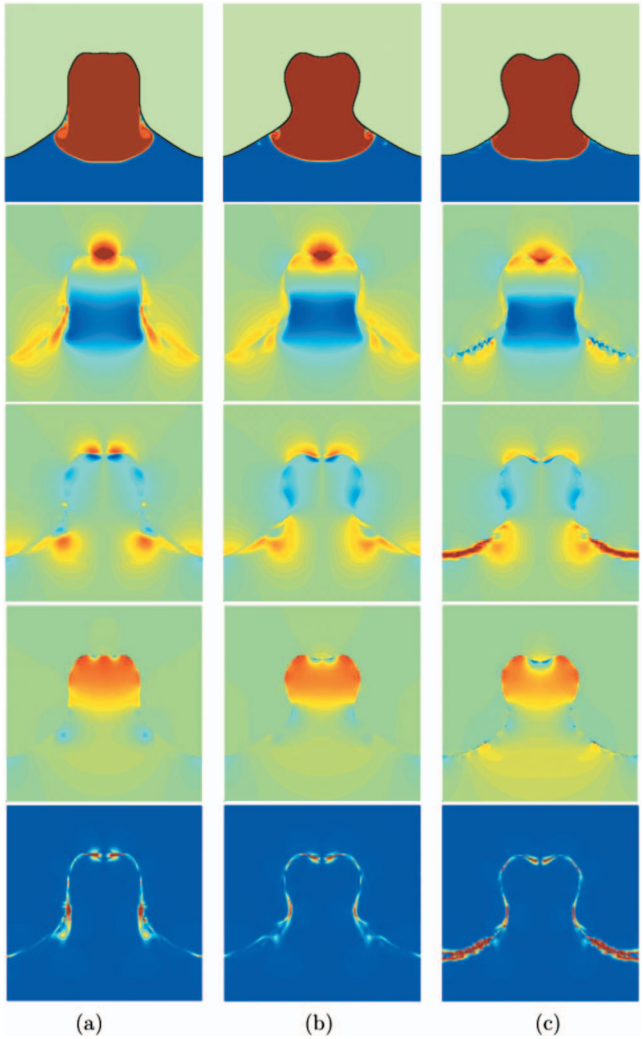

FIG. 5. (Color) Snapshots of the flow of a coalescing drop at time $t=0.8$ with (a) $R_\sigma=0.92$, (b) $R_\sigma=1$, and (c) $R_\sigma=1.5$. Top row: the concentration of liquid 1 (red) and 2 (blue). Row 2: the vertical velocity (red is upward, blue downwards). Row 3: the radial velocity (red indicates radial flow away from the center, blue toward the center). Row 4: the pressure (red is high and blue is low). Bottom row: the magnitude of the tangential stress (red is high and blue low).

The evolution of the various energy components is shown in Fig. 4(c). Initially, the excess surface energy (relative to that of a flat surface of the liquid of lowest surface tension) accounts for all the available energy. At early times, surface energy is transferred to kinetic energy and dissipated through the action of viscosity at approximately equal rates. Closer to pinch-off, the surface area of the drop and associated surface energy increase slightly, while the kinetic energy decreases. The increase in the concentration of liquid 1 at the interface due to diffusive effects results in a significant transfer of the available energy, up to 15%, from the internal energy of the bulk fluid into surface energy. Simulations performed with various Schmidt numbers, $\mathrm{Sc}=\mu_l/\rho_l\kappa$, all showed a similar transfer. Larger values of R_σ lead to even larger energy transfers, up to 40% for a ratio of $R_\sigma=1.5$. Because such transfers take place across a thin boundary layer under the interface, accurately modeling them requires higher resolutions. The conservation of total energy worsens

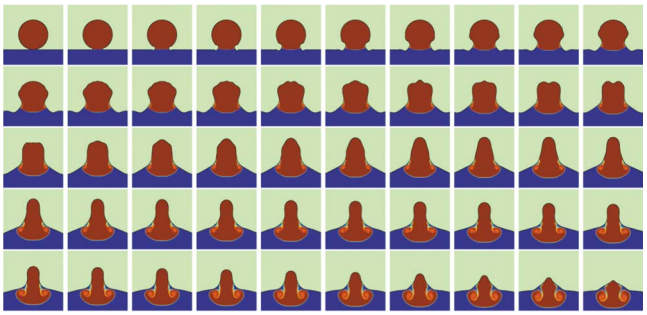

FIG. 6. (Color online) Simulation of the coalescence of a drop of larger surface tension than that of the reservoir, $R_\sigma=\sigma_2/\sigma_1=0.92$. Each image shown is 0.04 nondimensional time units apart. Despite the low Ohnesorge number, $\mathrm{Oh}=0.001$, the surface tension variations prevent partial coalescence.

with increasing R_σ, but it remained better than 90% for surface tension ratios as large as $R_\sigma=1.5$ at the resolution used throughout our study, $N=1024$. In the regime $0.66\leq R_\sigma \leq 1.5$, our simulations are therefore sufficiently accurate to provide a reliable description of the drop coalescence.

We show in Fig. 5 snapshots of the concentration, velocities, pressure, and tangential stress fields for different values of the surface tension ratio. Although all the plots correspond to the same nondimensional time, the evolution of the coalescence is more advanced for drops of larger R_σ. In all cases, the stresses are confined to a thin region near the interface. The most important difference to note between the different values of R_σ is the tangential motion present along the interface, inward in sequence (a) where $R_\sigma<1$ and outward in sequence (c) where $R_\sigma>1$. We note that the region of high pressure present near the tip of the drop is largest in the case $R_\sigma<1$, which is likely to accelerate the downward motion of the drop fluid, an observation we investigate further in Sec. V B.

B. Coalescence process

The evolution of the coalescence process is shown in Figs. 6–9 for $R_\sigma=\sigma_2/\sigma_1$ equal to 0.92, 0.967, 1, and 1.5, respectively. In the online version, the drop and reservoir liquids and the outside gaseous phase are initially maroon, blue, and green, respectively, while they are pale gray, dark

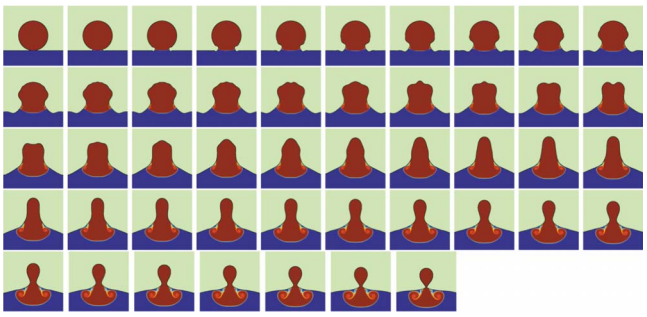

FIG. 7. (Color online) Simulation of the coalescence of a drop with slightly larger surface tension than the reservoir, $R_\sigma=\sigma_2/\sigma_1=0.9667$. Each image shown is 0.04 nondimensional time units apart and $\mathrm{Oh}=0.001$. Partial coalescence is observed, although the drop is smaller than it would be in the absence of the surface tension mismatch.

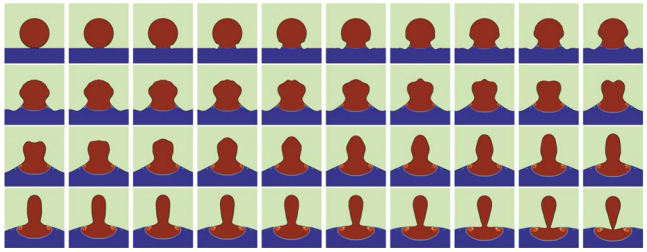

FIG. 8. (Color online) Simulation of the coalescence of a drop with surface tension equal to that of the reservoir, $R_\sigma=\sigma_2/\sigma_1=1$. Each image shown is 0.04 nondimensional time units apart and Oh=0.001.

gray, and white in the print version, with regions of mixed liquids appearing as white. The Ohnesorge number was chosen sufficiently small, Oh=0.001, to ensure that viscous dissipation is negligible. The radius of the computational domain was chosen to be sufficiently large, $6R$, to ensure that boundaries played no role in the coalescence process; in particular, it was much larger than the domain shown in Figs. 6–9.

We compare the coalescence of liquids of identical surface tension to that of liquid of uneven surface tensions. Whenever $R_\sigma \neq 1$, the region of higher surface tension pulls on the interface and generates a tangential flow that partially coats the surface of the liquid of largest surface tension with the second fluid. Zooming in on the interface at the point where the drop and reservoir liquids meet clearly shows the tangential motion (Fig. 10), and the tiny eddy it generates just below the interface. To provide a local measure of the Reynolds number resulting from such tangential flows, Re_i, we estimate the thickness of the fluid layer entrained by the tangential surface flow as $\delta \sim \sqrt{\mu_l \tau/\rho_l}$, with $\tau=(\rho_l R^3/\sigma)^{1/2}$ the characteristic coalescence time scale, and the tangential velocity by balancing characteristic tangential Marangoni and viscous stresses to find $U \sim \Delta\sigma/\mu_1(\delta/R)$. We thus estimate $\mathrm{Re}_i=U\delta\rho_l/\mu_l=\mathrm{Oh}^{-1}\ \Delta\sigma/\sigma$, which in the cases shown in Fig. 10 yields $\mathrm{Re}_i \sim 50$. Even over such a small length scale, tangential motion may thus generate vigorous vortices.

As can be seen by comparing the final images of Figs. 7–9, the coalescence process is much more sensitive to the surface tension ratio for $R_\sigma<1$ than for $R_\sigma>1$. For drops such that $R_\sigma>1$, the tangential motion causes the drop fluid

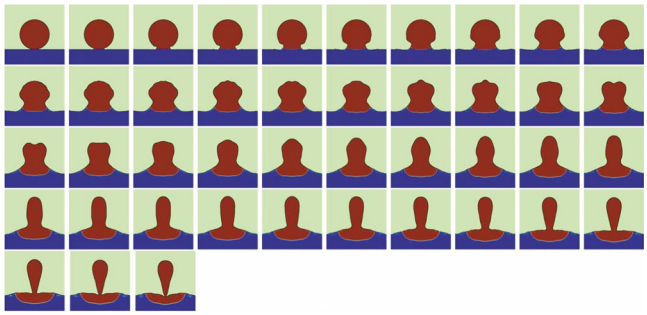

FIG. 9. (Color online) Simulation of the coalescence of a drop with lower surface tension than the reservoir, $R_\sigma=\sigma_2/\sigma_1=1.5$. Each image shown is 0.04 nondimensional time units apart and Oh=0.001. Tangential motion along the interface is away from the drop, which prevents the detachment of the vortex ring.

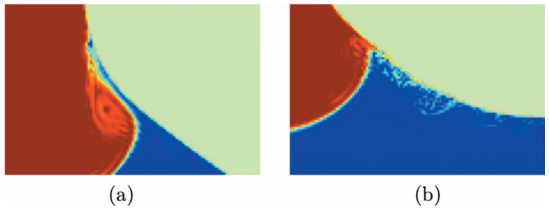

FIG. 10. (Color online) Evidence of tangential motion generated by surface tension mismatch for (a) $R_\sigma=\sigma_2/\sigma_1=0.9667$ and (b) $R_\sigma=1.5$. Both images were taken at a nondimensional time of $t=0.76$ after the onset of coalescence and have a Ohnesorge number of 0.001. The same full picture of the drop can be seen in the 20th frame of Figs. 7 and 9. Note the vortex evident in (a).

to spread over the reservoir, a process which does not directly influence the competition between pinch-off and vertical collapse. Coalescence then progresses in a manner very similar to when $R_\sigma=1$. However, when $R_\sigma<1$, the tangential motion along the interface brings fluid of lower surface tension up the sides of the drop. The interface driving the horizontal constriction therefore has a diminished surface tension. The horizontal constriction is then slowed (Fig. 7), and the vertical collapse dominates, expelling fluid downward. If R_σ is sufficiently close to 1, the sides of the drop are eventually covered with the larger surface tension fluid, and pinch-off may then occur. The resulting partial coalescence thus occurs at a later time and the resulting daughter drop is smaller and made up nearly entirely of the same fluid as the mother drop. A drop with $R_\sigma<1$ also causes the vortex ring created as fluid is expelled into the bath to detach from the interface. Vortex detachment can also occur in homogeneous coalescence but our simulations show that it requires a significantly smaller Ohnesorge number.

We also performed simulations with Schmidt numbers $\mathrm{Sc}=\nu_1/\kappa$ ranging from 1 to 50, which encompass the regime where temperature variations cause surface tension variations, the Schmidt number then playing the role of the Prandtl number. The observed coalescence showed very little dependence on Sc and the main features described above were reproduced. We also attempted to simulate coalescence in conditions resembling those of the last sequences of pictures shown in Fig. 2, with $R_\sigma<0.5$. In this regime, we found that accurately representing the dynamics of the thin layer of outer fluid required far higher resolutions, and we could not investigate numerically the regime where drop ejections were observed in our experiments.

VI. DISCUSSION

The influence of surface tension variations on drop coalescence is summarized in Fig. 11. Partial coalescence in the ordinary sense is only possible when $R_\sigma>0.93$. In that regime, we find a critical value of Oh_c below which partial coalescence occurs [Fig. 11(a)]. To determine numerically the value of Oh_c, we fix all other parameters and systematically vary the Ohnesorge number, using a bisection method to accurately determine Oh_c. In regions where the slope of Oh_c as a function of the surface tension becomes large, we reverse the procedure by fixing Oh and varying the surface

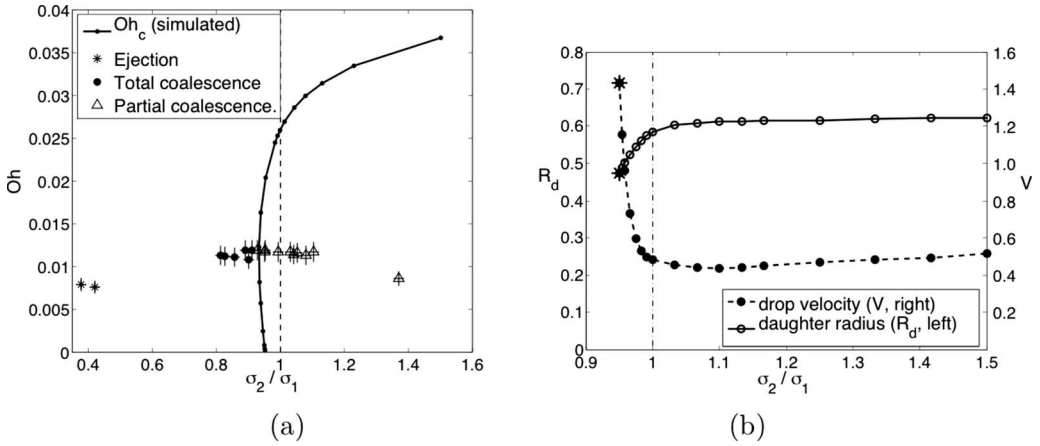

FIG. 11. (a) Coalescence in ethanol/water mixtures. The solid line shows the numerically computed critical value of the Ohnesorge number, Oh_c, below which partial coalescence may occur, as a function of surface tension R_σ, while the symbols are experimental results. (b) Dependence of the daughter drop radius (left) and velocity (right) on the surface tension ratio. Here the Ohnesorge number was kept constant at Oh=0.001 to keep viscous effects to a minimum.

tension ratio. When the surface tension of the reservoir is less than that of the drop, partial coalescence is hindered and Oh_c quickly goes to zero. However, using a drop of weaker surface tension than the reservoir only slightly increases Oh_c. Our simulations have not yielded any partial coalescence for $Oh > 0.04$, regardless of the choice of R_σ.

For $R_\sigma < 1$, quite surprisingly, Oh_c increases nonmonotonically with R_σ. Our observations suggest that viscous effects act to both damp capillary waves and slow the spread of the low surface tension fluid at the interface. At very low values of Oh, the hindering of tangential flow by viscous effects is dominant, and increasing Oh therefore facilitates partial coalescence. However, for $Oh > 0.02$, the damping of capillary waves by viscous effects becomes dominant, and so favors total coalescence.

The daughter drop size and velocity are strongly affected when $R_\sigma < 1$. Figure 11(b) shows the daughter drop radius and velocity at a fixed Ohnesorge number Oh=0.001 for given surface tension ratios. We first note that the daughter drop radii are only weakly affected by surface tension variations. The smallest drops are generated when $R_\sigma = 0.93$ and have radii as small as 0.47. Figure 11(b) shows the droplet fluid's average downward velocity at the moment of pinch-off. The time of pinch-off, not shown, follows a curve similar to that of the daughter drop velocity, but with far less variation, with pinch-off times of 1.94, 1.63, and 1.71 at surface tension ratios of $R_\sigma = 0.93, 1$, and 1,5, respectively (see Figs. 7–9). Longer pinch-off times allow the daughter droplets to gather more downward momentum before being released to bounce on the reservoir surface, hence the similarity of the pinch-off time and velocity curves. We note that drops of larger surface tension than the reservoir can reach velocities more than twice that of a drop of the same composition as the reservoir, and thus potentially bounce up to four times higher.

A striking feature of partial coalescence is the coalescence cascade that occurs as the daughter droplets become progressively smaller. We proceed by discussing how this cascade is affected by a compositional difference between drop and bath. We observed coalescence cascades for drops having surface tension smaller than that of the reservoir ($R_\sigma \geq 1$). Figure 9 illustrates that typically, only the first coalescence event of the cascade would be influenced by the surface tension mismatch. Unless the daughter drop drifted sideways significantly (which does occasionally happen), the second coalescence event would be between a drop and reservoir of local composition identical to that of the drop. As the first daughter drop size is only weakly affected by the surface tension gradient, earlier descriptions of partial coalescence[10] are therefore also relevant when $R_\sigma > 1$.

Daughter drops issued from the partial coalescence of drops with $R_\sigma < 1$ appear to have a composition identical to that of the mother drop. However, surface tension gradients favor the detachment from the interface of the vortex ring formed during coalescence; thus, any daughter drop would encounter a reservoir with a surface tension nearly equal to that of the original reservoir (see Fig. 7). The lower critical Ohnesorge number of coalescence associated with $R_\sigma < 1$, combined with the progressively smaller size of the daughter droplets, thus restricts the coalescence cascade to a very narrow parameter regime.

The presence of surface active reagents (surfactants) on the interface also alters surface tension, and varying concentrations generally lead to surface tension gradients.[38] Because such molecules, when insoluble, are surface bound, expansion or contraction of the interface affects their concentration, thus contributing an effective elasticity to the interface, an aspect not considered here. We note that the most important contraction of the interface occurs in the early stages of coalescence, at the opening of the neck. If surfactants are present, such a contraction will increase their concentration, and so typically reduce surface tension. In light of the current results, we anticipate that surfactant-laden interfaces would therefore tend to favor total coalescence, as the horizontal pull of surface tension would be weakened by the larger concentration of surfactants accumulating around the neck of the drop. As a caveat, we note that such a prediction remains a conjecture.

VII. CONCLUSION

We have presented the results of a combined experimental and numerical investigation of drop coalescence into a reservoir in the presence of Marangoni stresses. Vigorous tangential motions generate eddies lying tangent to the interface. Drops of smaller surface tension than the reservoir are only weakly affected by the tangential motion due to the surface tension mismatch. Conversely, the conditions under which drops of larger surface tension undergo partial coalescence are strongly restricted by the intrusive surface motion of the reservoir fluid. The surface tension along the sides of the drop is then diminished, and the total coalescence driven by the curvature at the top of the drop is favored. When partial coalescence did occur ($R_\sigma > 0.93$), the size of the resulting daughter drops increased with increasing R_σ. The converging surface flow arising for $R_\sigma < 1$ favored the detachment from the surface of the vortex ring formed during coalescence, while the diverging flow arising for $R_\sigma > 1$ hindered its detachment.

We also discovered a different type of droplet ejection prompted by the convergence of tangential surface motion driven by Marangoni stresses. This type of ejection differs from the typical partial coalescence in that it generates significantly smaller drops, with approximately a tenth radius of the mother drop. Our numerical methods were insufficiently refined to replicate such ejections, but we are hopeful that improved methods will soon be able to accurately model the thin boundary layer then present near the interface, and thus to capture drop ejection resulting from converging surface flows.

Our results provide a description of drop coalescence when drops and reservoirs are not necessarily identical, isothermal fluids. In particular, we may now explain the observation of Ref. 9 that partial coalescence was more difficult to observe in a repeatable manner using water as the reservoir and drop liquid. Water left standing quickly becomes contaminated with dust particles that decrease its surface tension. In contrast, a newly formed drop is likely to have a clean surface with a relatively high surface tension. The effective surface tension ratio is therefore likely to satisfy $R_\sigma < 1$, which restricts the conditions under which partial coalescence may arise. While the same effects are likely to come into play for fluids of lower surface tension such as oils, they will be less significant owing to the relative insensitivity of such fluids to surface contamination.

ACKNOWLEDGMENTS

F.B. was supported by the NSF under DMS Applied Mathematics Grant No. 0808129.

[1] A. Bhakta and E. Ruckenstein, "Decay of standing foams: Drainage, coalescence and collapse," Adv. Colloid Interface Sci. **70**, 1 (1997).
[2] E. X. Berry and R. L. Reinhardt, "Analysis of cloud drop growth by collection. 3. Accretion and self-collection," J. Atmos. Sci. **31**, 2118 (1974).
[3] H. A. Stone, A. D. Stroock, and A. Ajdari, "Engineering flows in small devices: Microfluidics toward a lab-on-a-chip," Annu. Rev. Fluid Mech. **36**, 381 (2004).
[4] O. D. Velev, B. G. Prevo, and K. H. Bhatt, "On-chip manipulation of free droplets," Nature (London) **426**, 515 (2003).
[5] J. J. Thomson and H. F. Newall, "On the formation of vortex rings by drops falling into liquids, and some allied phenomena," Proc. R. Soc. London **39**, 417 (1885).
[6] A. V. Anilkumar, C. P. Lee, and T. G. Wang, "Surface-tension-induced mixing following coalescence of initially stationary drops," Phys. Fluids A **3**, 2587 (1991).
[7] G. E. Charles and S. G. Mason, "The mechanism of partial coalescence of liquid drops at liquid/liquid interfaces," J. Colloid Sci. **15**, 105 (1960).
[8] G. E. Charles and S. G. Mason, "The coalescence of liquid drops with flat liquid/liquid interfaces," J. Colloid Sci. **15**, 236 (1960).
[9] F. Blanchette and T. P. Bigioni, "Partial coalescence of drops at liquid interfaces," Nat. Phys. **2**, 254 (2006).
[10] S. T. Thoroddsen and K. Takehara, "The coalescence cascade of a drop," Phys. Fluids **12**, 1265 (2000).
[11] X. Chen, S. Mandre, and J. J. Feng, "Partial coalescence between a drop and a liquid-liquid interface," Phys. Fluids **18**, 051705 (2006).
[12] P. Pikhitsa and A. Tsargorodskaya, "Possible mechanism for multistage coalescence of a floating droplet on the air/liquid interface," Colloids Surf., A **167**, 287 (2000).
[13] H. Aryafar and H. P. Kavehpour, "Drop coalescence through planar surfaces," Phys. Fluids **18**, 072105 (2006).
[14] T. Gilet, K. Mulleners, and J. P. Lecomte, "Critical parameters for the partial coalescence of a droplet," Phys. Rev. E **75**, 036303 (2007).
[15] E. M. Honey and H. P. Kavehpour, "Astonishing life of a coalescing drop on a free surface," Phys. Rev. E **73**, 027301 (2006).
[16] J. Thomson, "On certain curious motions observable on the surfaces of wine and other alcoholic liquours," Philos. Mag. **10**, 330 (1855).
[17] C. Marangoni, "Ueber die ausbreitung der tropfen einer flüssigkeit auf der oberfläche einer anderen (On the expansion of a drop of fluid on the surface of another)," Ann. Phys. Chem. **219**, 337 (1871).
[18] T. D. Hodgson and J. C. Lee, "The effect of surfactants on the coalescence of a drop at an interface," J. Colloid Interface Sci. **30**, 94 (1969).
[19] T. D. Hodgson and D. R. Woods, "The effect of surfactants on the coalescence of a drop at an interface ii," J. Colloid Interface Sci. **30**, 429 (1969).
[20] P. Dell'Aversana, J. R. Banavar, and J. Koplik, "Suppression of coalescence by shear and temperature gradients," Phys. Fluids **8**, 15 (1996).
[21] G. P. Neitzel and P. Dell'Aversana, "Noncoalescence and nonwetting behavior of liquids," Annu. Rev. Fluid Mech. **34**, 267 (2002).
[22] S. T. Thoroddsen, B. Qian, T. G. Etoh, and K. Takehara, "The initial coalescence of miscible drops," Phys. Fluids **19**, 072110 (2007).
[23] Y. Couder, E. Fort, C. H. Gauthier, and A. Boudaoud, "From bouncing to floating: Noncoalescence of drops on a fluid bath," Phys. Rev. Lett. **94**, 177801 (2005).
[24] T. Gilet, N. Vandewalle, and S. Dorbolo, "Controlling the partial coalescence of a droplet on a vertically vibrated bath," Phys. Rev. E **76**, 035302 (2007).
[25] H. Aryafar and H. P. Kavehpour, "Hydrodynamic instabilities of viscous coalescing droplets," Phys. Rev. E **78**, 037302 (2008).
[26] K. R. Sreenivas, P. K. De, and J. H. Arakeri, "Levitation of a drop over a film of flow," J. Fluid Mech. **380**, 297 (1999).
[27] R. C. Ernst, C. H. Watkins, and H. H. Ruwe, "The physical properties of the ternary system ethyl alcohol-glycerin-water," J. Phys. Chem. **40**, 627 (1936).
[28] L. Duchemin, S. Popinet, C. Josserand, and S. Zaleski, "Jet formation in bubbles bursting at a free surface," Phys. Fluids **14**, 3000 (2002).
[29] S. T. Thoroddsen, T. G. Etoh, and K. Takehara, "Microjetting from wave focusing on oscillating drops," Phys. Fluids **19**, 052101 (2007).
[30] Y. Renardy, S. Popinet, L. Duchemin, M. Renardy, S. Zaleski, C. Josserand, M. A. Drumright-Clarke, D. Richard, C. Clanet, and D. Quéré, "Pyramidal and toroidal water drops after impact on a solid surface," J. Fluid Mech. **484**, 69 (2003).
[31] A. Prosperetti and H. N. Oguz, "The impact of drops on liquid surfaces and the underwater noise of rain," Annu. Rev. Fluid Mech. **25**, 577 (1993).
[32] F. Blanchette and T. P. Bigioni, "Dynamics of drop coalescence at fluid interfaces," J. Fluid Mech. **620**, 333 (2009).
[33] J. U. Brackbill, D. B. Kothe, and C. Zemach, "A continuum method for modeling surface tension," J. Comput. Phys. **100**, 335 (1992).
[34] B. Lafaurie, C. Nardone, R. Scardovelli, S. Zaleski, and G. Zanetti, "Modelling merging and fragmentation in multiphase flows with surfer," J. Comput. Phys. **113**, 134 (1994).

[35]S. Popinet and S. Zaleski, "A front tracking algorithm for the accurate representation of surface tension," Int. J. Numer. Methods Fluids **30**, 775 (1999).
[36]F. Blanchette and Y. Lei, "Energy considerations for multiphase fluids with variable density and surface tension," SIAM Rev. **51**, 423 (2009).
[37]D. L. Brown, R. Cortez, and M. L. Minion, "Accurate projection methods for the incompressible Navier–Stokes equations," J. Comput. Phys. **168**, 464 (2001).
[38]P. G. De Gennes, F. Brochard-Wyart, and D. Quéré, *Gouttes, Bulles, Perles et Ondes* (Belin, Paris, 2002), Chap. 8.